Towards the Discrimination between Natural and Synthetic Pigments: The Case of Ultramarine

Anastasia Pourliaka [*] **, Lamprini Malletzidou, Triantafillia Zorba, Konstantinos M. Paraskevopoulos, Eleni Pavlidou and George Vourlias**

Laboratory of Advanced Materials & Devices, School of Physics, Faculty of Sciences, Aristotle University of Thessaloniki
Thessaloniki, GR-54124, Greece

E-mail: apourlia@physics.auth.gr, labrinim@auth.gr, zorba@auth.gr, kpar@auth.gr, elpavlid@auth.gr, gvourlia@auth.gr

Ultramarine has been for centuries one of the most highly prized pigments of all traditional artists' materials, due to its durability, excellent color, and its intrinsic value. For the production of the blue pigment Ultramarine, the rare semiprecious stone Lapis Lazuli has been used, found since ancient times in mines northeast of Afghanistan, making it difficult to transport to the Mediterranean region. Since 1828, when the synthetic form was discovered, it has become widely used and synthetic Ultramarine blue has replaced the natural variety in painting palettes. Therefore, one key objective in authentication issues is to distinguish between natural and synthetic Ultramarine. In this research work, ten commercial Ultramarine pigments - of both natural and synthetic origin- were used to investigate the possibility of their discrimination using various characterization methods. The pigments were studied by Fourier transform infrared (FTIR) spectroscopy, X-ray diffractometry (XRD), electron microscopy (SEM-EDS), and UV-Vis spectrophotometry. The combination of elemental composition, morphological analysis, phase identification, color calculation, and optical band gap estimation is used, towards an analytical protocol for the discrimination between samples of synthetic and natural origin.

11th International Conference of the Balkan Physical Union (BPU11),
28 August - 1 September 2022
Belgrade, Serbia

---

[*] Speaker

1.   Introduction

Among pigments used for painting purposes, Ultramarine -derived from the rare semiprecious stone lapis lazuli- has been considered for centuries one of the most highly prized ones, due to its durability, excellent color, and its intrinsic value. Lapis lazuli has been mined since ancient times in mines northeast of Afghanistan, making it difficult to be transported to the Mediterranean region. The first known use of lapis lazuli pigment dates back to the 6th and 7th centuries AD, in paintings of cave temples in Afghanistan [1]. Ultramarine was a very expensive and precious blue pigment extensively used in Europe throughout the 14th and 15th centuries in mediaeval paintings and frescoes. This precious pigment took on an iconographic value and it was reserved for the robes of only the most prominent figures, such as Christ and the Virgin Mary in religious scenes. The production of a synthetic version by Guimet in 1828, which was obtained from the calcination of a mixture of metakaolin, sulphur, sodium carbonate, and a reducing agent, followed by an oxidation step, has introduced an important change in artists' habits, in that a less expensive pigment was available for their palettes.

The mineral responsible for the blue color of lapis lazuli is lazurite ($Na_8Al_6Si_6O_{24}Sn$), a member of the aluminosilicate group, with the same structure as sodalite ($Na_8Al_6Si_6O_{24}Cl_2$). Ultramarine has the highly reactive radical ions S_2^- and S_3^- which, according to molecular orbital theory, must contain unpaired electrons and are only stabilized by their occupancy of the aluminosilicate framework. The radical anions have been detected by their electron spin resonance spectra, while theoretical calculations indicate the importance of S_3^- in producing the blue color in lapis lazuli [2]. Depending on the location of the rock's origin, natural lazurite can be found in combination with other minerals such as calcite ($CaCO_3$), pyrite (FeS_2) [3], diopside ($CaMgSi_2O_6$), phlogopite ($K(Mg,Fe,Mn)_3Si_3AlO_{16}(F(OH)_2)$), wollastonite ($CaSiO_3$) [4], forsterite ($Mg_2SiO_4$), and muscovite ($KAl_2(Al\text{-} Si_3O_{10}) (OH)_2$) [2, 3]. Lazurite is a sulfur-containing variant of the closely related minerals haüyne and nosean, which are members of the sodalite group of feldspathoid framework silicates [5].

The presence of out-of-date modern pigments, such as synthetic Ultramarine blue, in old paintings may be especially interesting for problems of authentication or for spotting unidentified later restoration efforts. Finding additional minerals and impurities that are absent from synthetic pigments but present in natural ones requires the employment of various characterization techniques.

Nevertheless, researchers at the Getty Conservation Institute (GCI) first observed a strong vibrational band of unknown origin in the Fourier transform infrared (FTIR) spectra of a natural Ultramarine pigment from Afghanistan, collected from an Italian painting from the 16th century [6]. This band, located at 2340 cm^{-1}, and later attributed to entrapped CO_2, is not present in the spectra of the synthetic Ultramarines and can be used to identify natural Ultramarine of Afghanistan [7]. However, the 2340 cm^{-1} feature cannot serve as a specific indicator of a geological source for lapis lazuli. As confirmed by Smith and Klinshaw, this band that is associated with CO_2 entrapped into natural lazurite, but it is not reported in every natural Ultramarine of geological origin [8]. Moreover, the distinction between natural and synthetic Ultramarine using conventional FTIR spectroscopy which does not operate in vacuum mode is difficult, as the bands of interest coincide with those of atmospheric CO_2 (2400-2300 cm^{-1}).

The present work is focusing in the characterization of commercial natural and synthetic Ultramarine, to propose an analytical approach towards the discrimination of the pigment's origin and provenance.

2.   Experimental section

2.1 Pigment Samples

Ten Ultramarine blue pigments in powder form were purchased from Kremer Pigmente GmbH & Co. KG (Germany). Their order number and description are included in Table 1. The pigments under study include three natural samples of different qualities (prefix NAT), as well as seven synthetic ones (prefix SYN). Regarding the ones of natural origin, they had been prepared from lapis lazuli rock according to traditional procedures, as stated by the supplier [9].

Sample	Order No.	Pigment	Composition
SYN-1	4500	Ultramarine Blue, very dark	Synthetic pigment
SYN-2	4508	Ultramarine blue, light	Synthetic pigment
SYN-3	45010	Ultramarine Blue, dark	Synthetic pigment
SYN-4	99750	Ultramarine Blue, Belgian	Synthetic pigment (Historical stock)
SYN-5	45020	Ultramarine Blue, reddish	Synthetic pigment
SYN-6	45040	Ultramarine Blue, greenish light	Synthetic pigment
SYN-7	45030	Ultramarine Blue, greenish extra	Synthetic pigment
NAT-1	1052	Lapis Lazuli, good quality	Natural Ultramarine, Afghanistan
NAT-2	1056038	Lapis Lazuli	Natural Ultramarine, Chile
NAT-3	10550	Lapis Lazuli, bright pure blue	Natural Ultramarine, South America

Table 1: The pigments under study.

2.2. Instrumentation

Fourier Transform Infrared (FTIR) spectroscopy was applied for the characterization of the ten pigment samples, using a Perkin Elmer spectrometer, model Spectrum 1000. The spectra were collected in the MIR region (4000 - 400 cm^{-1}), in transmittance mode, with 32 scans and a 4 cm^{-1} resolution.

X-ray diffraction (XRD) analysis was carried out using with a two-cycle Rigaku diffractometer, model Ultima^{+} -operating at 40 kV/30 mA with Cu K_α radiation (λ= 0.154 nm). Measurements were performed in the range of 5–90°, with a step of 0.05° and scan speed of 1°/min. The Rietveld analysis was performed using the free and open-source FullProf Suite application (version January 2021). As a database, the model data were used diffraction tables (PDF) of the ICDD application (International Center of Diffraction Data).

The elemental and surface morphological study of the pigments was performed with a JEOL scanning electron microscope (SEM), model JSM 7610 F PLUS, with an integrated OXFORD AZTEC X-ray Energy Dispersive Spectrometer (EDS), with operating conditions: accelerating voltage 15-20 kV and a working distance of 8 mm. The samples were carbon-coated before their study.

UV-Vis measurements were carried out on with a Perkin Elmer spectrophotometer, model Lambda 18, in diffuse reflectance mode, in the spectral region of 200 - 800 nm, using a $BaSO_4$

covered integrating sphere. The measurements were used to determine the exact color of the pigments and to calculate their optical band gap.

3.   Results and Discussion

3.1. FTIR spectroscopy

In the first stage of the project, all samples were measured by FTIR spectroscopy. The differences between the spectra of natural and synthetic Ultramarines (Fig. 1) are related to the presence of kaolinite in the synthetic pigments, whereas in the natural pigments the difficulty to locate the S_3^- chromophore is evident. In particular, Fig. 1a depicts the FTIR spectra of the synthetic pigments, and kaolinite ($Al_2(OH)_4Si_2O_5$) is found to be present mostly from its characteristic FTIR bands at 3698 and 3618 cm^{-1}, as the bands at 1150 – 1000 cm^{-1} are generally attributed to Si-O and Al-O of silicates and aluminosilicates [10]. As a result, kaolinite's bands in this spectral region are overlapped by the pigments' other components. Following this, the bands at 1012, 1150, 697, 660 and 450 cm^{-1} are reported as characteristic Ultramarine framework bands of the sodalite structure [7, 11, 12]. Additionally, the light-colored pigments are characterized by the presence of calcite, because of the bands at 2512, 1796, 1550-1350, 877 and 712 cm^{-1} [13]. The weak band at 584 cm^{-1} is attributed to the ν_3 stretching vibration of the blue chromophore S_3^-, which is evident in the spectra of all the synthetic pigments, but is difficult to be distinguished due to band overlapping in the ones of natural origin (Fig. 1b).

In the case of the natural pigments, the characteristic Ultramarine framework bands are repeated at 1003 cm^{-1}, enhanced by a shoulder at 1150 cm^{-1} due to the stretching of the Si-O tetrahedra of the aluminosilicate composition. Moreover, there is the presence of the bands at 645 and 568 cm^{-1} due to Al-O stretching of $(Al_6Si_6)O_{24}$, along with a strong band at 450 cm^{-1} due to Si-O-Al [11]. Additionally, there is a small presence of calcite in sample NAT-1, due to the characteristic FTIR bands at ~1450 and 874 cm^{-1}. Finally, the broad bands of low intensity, that appear at 3434 and 1630 cm^{-1} in most samples, are attributed to the vibrations of the hydroxyl groups [14].
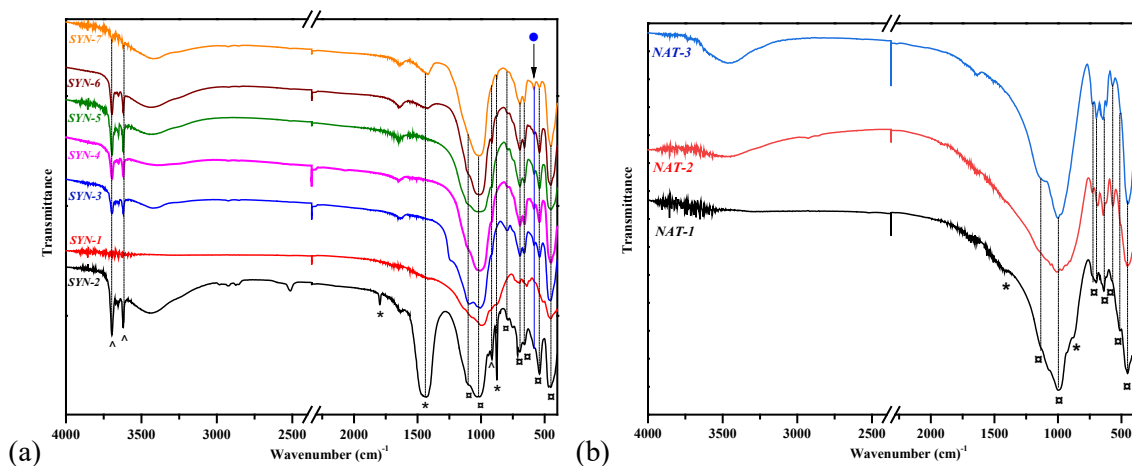
Figure 1: *FTIR spectra of (a) the synthetic and (b) natural pigments (* calcite, ^ kaolinite, ¤ aluminosilicates, and • S_3^- ion).*

3.2 X-ray Powder Diffraction
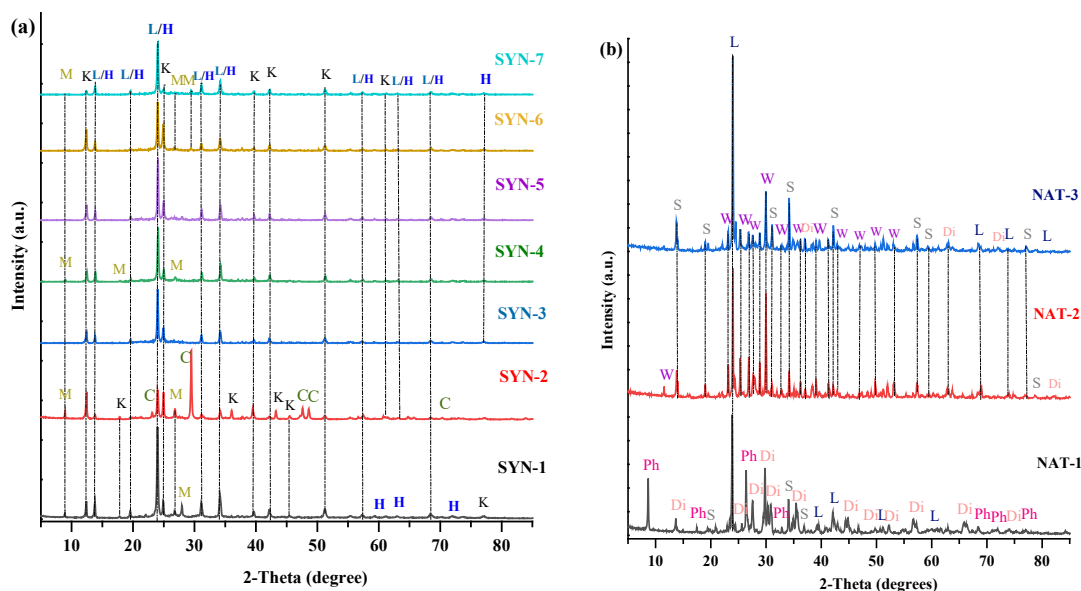
Figure 2: *X-Ray diffractograms of (a) synthetic and (b) natural origin pigment samples. L: Lazurite, H: haüyne, K: Kaolinite, C: Calcium Carbonate, M: Muscovite, Ph: Phlogopite, S: Sodalite, W: Wollastonite and Di: Diopside*

XRD analysis was applied towards the better understanding of the crystalline phases that are present in the synthetic and natural pigments (Fig. 2). For all the pigments, phase identification and quantitative assessments were performed (Fig. 3) [15]. Lazurite, haüyne, kaolinite, muscovite and calcite are the major phases in the synthetic pigments, as it is shown in Fig. 2a. The phase identification was performed with the following PDF cards: Lazurite cubic #77-1702, lazurite cubic #77-1703, haüyne cubic #73-1920, kaolinite triclinic #78-2109, kaolinite 2M monoclinic #75-0938, muscovite-2M2 monoclinic #34-0175 and calcium carbonate hexagonal #85-1108 [16]. Lazurite and haüyne are the two primary phases depicted in the pattern (Fig 2a, Fig. 3). Less prominently shown phases include kaolinite and muscovite. The study of the previous experimental method (3.1) confirms the existence of kaolinite, and muscovite is a common phase alongside lazurite and haüyne.

Regarding the pigments of natural origin, their present primary phases that vary in ratio, according to the raw material's extraction location [5], as presented in Fig. 2b and Fig. 3. The principal phases contained in sample NAT-1, which originates from mineral lapis lazuli from Afghanistan, are lazurite, sodalite, diopside, and phlogopite. The other two pigments of natural origin (NAT-2 and NAT-3) which originate from South America, are composed of lazurite, wollastonite, sodalite, and diopside. The XRD patterns that were collected for all pigments of natural origin were identified using the PDF cards: Lazurite cubic #77-1703, phlogopite monoclinic #85-2275, sodalite cubic #82-1813, diopside monoclinic #81-0487 for NAT-1 and lazurite cubic #77-1703, sodalite cubic #82-1814, diopside monoclinic #71-1067, diopside monoclinic #83-1392 and wollastonite 1A triclinic #84-0654 for NAT-2 and NAT-3.
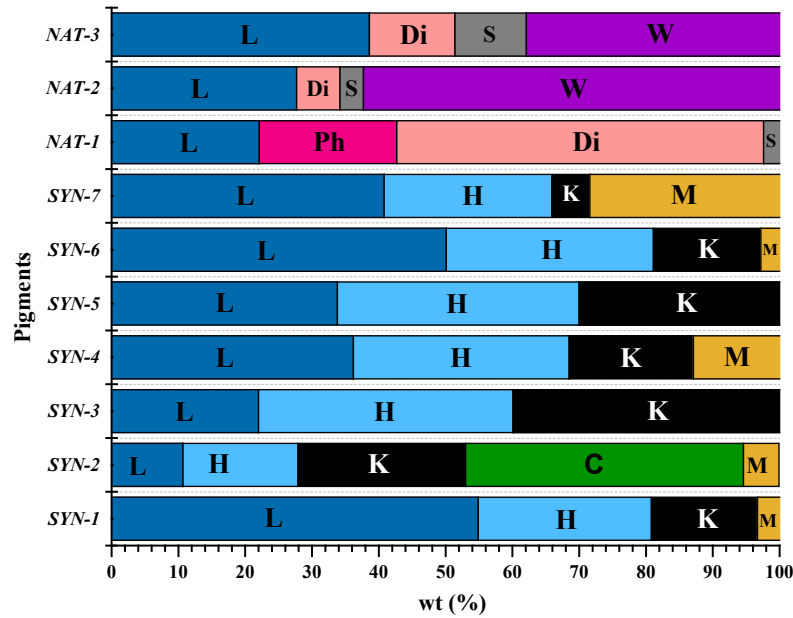
Figure 3: *Rietveld method quantification results of all the pigments. L: Lazurite, H: haüyne, K: Kaolinite, C: Calcium Carbonate, M: Muscovite, Ph: Phlogopite, S: Sodalite, W: Wollastonite and Di: Diopside*

3.3 SEM-EDS

The SEM-EDS analysis was used in order to obtain a detailed elemental analysis of all samples and the morphological characteristics of the pigments' grains. As is obvious from the SEM images between natural and synthetic pigments (Fig. 4 and Table 2), they differ in grain size and shape.

Sample	Average Grain Size (μm)	Standard Deviation (μm)
SYN-1	2.98	1.26
SYN-2	1.17	0.57
SYN-3	1.95	0.92
SYN-4	2.33	1.01
SYN-5	2.04	1.05
SYN-6	1.96	0.80
SYN-7	1.67	0.69
NAT-1	7.52	4.54
NAT-2	8.78	6.96
NAT-3	8.20	4.70

Table 2: *Average grain size and standard deviation of all Ultramarine pigments, as calculated from the collected SEM images.*

In particular, the pigments of synthetic origin exhibit homogeneous and spherical grains, as opposed to the pigments of natural origin derived from the mineral lapis lazuli, which exhibit larger grains with sharper edges. Moreover, NAT-1 -which originates from Afghanistan- presents an uneven grain surface and smaller grains than the other two natural pigments, which originate from lapis lazuli from Chile and South America (NAT-2 and NAT-3, respectively). This is supported by SEM images of individual lapis lazuli minerals from the two separate mining sites [5, 18]. NAT-2 is presented in three different magnifications in Fig. 4, as it presents inhomogeneity

regarding its grains. This can clearly be observed by Table 2, where the average grain size and its standard deviation are presented, as calculated from the collected SEM images; in every case, this calculation is based in ~150 different grains from each sample. The extremely high standard deviation -of ~50%- confirms the grain size inhomogeneity, especially in the natural pigments.
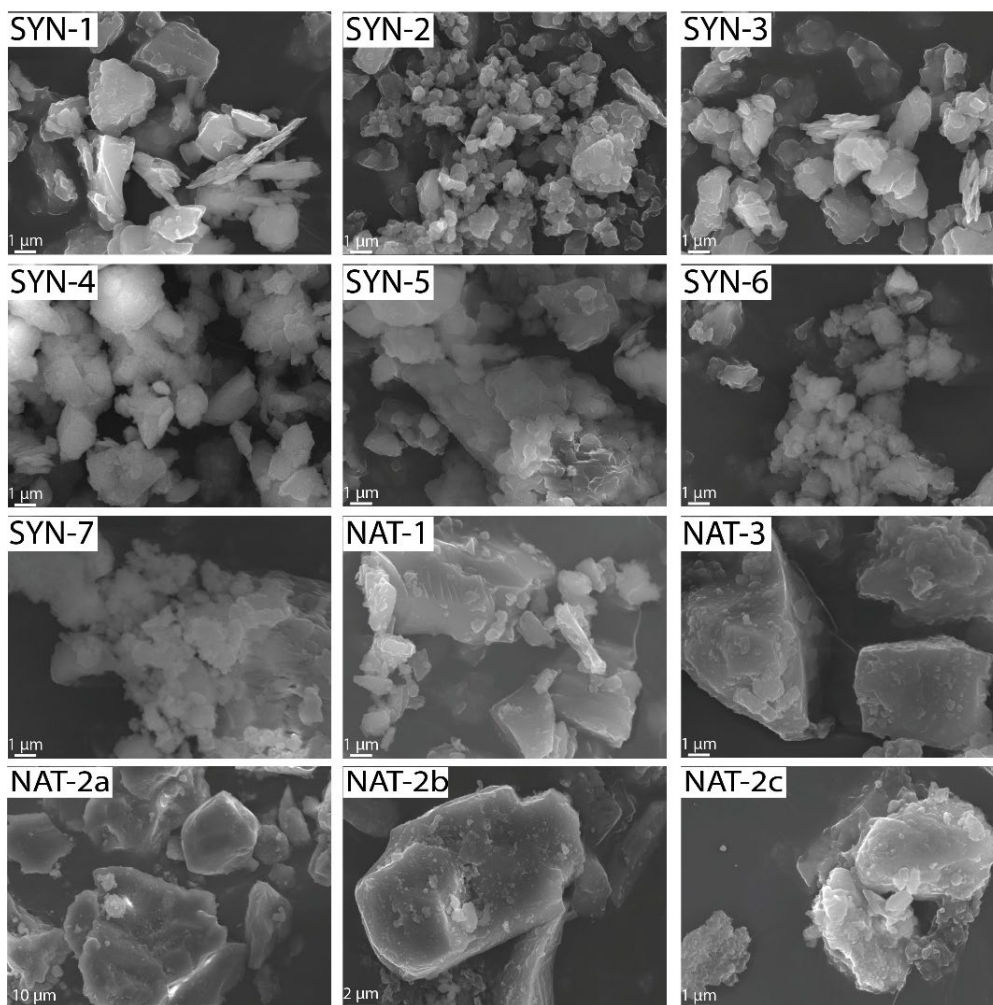
Figure 4: *Secondary electron SEM images for all Ultramarine pigments natural and synthetic origin*

As it can be seen in Table 3, the primary findings of the EDS investigation are supported by both the recovered crystalline phases from XRD and FTIR analyses [5, 17]. The main elements found in all pigments are oxygen, sodium, magnesium, aluminum, silicon, sulphur, potassium, calcium, and iron as shown by similar studies [18]. Additional elements like zirconium, nickel, phosphorus, bismuth, copper, and cerium are found in smaller amounts in synthetic pigment samples, probably as a result of sample contamination (Table 4). Likewise, samples of natural provenance once more exhibit low levels of contamination with elements like nickel, vanadium, phosphorus, and chromium. When comparing the two types of pigments, those from natural sources have higher percentages of calcium, silicon, magnesium, and iron due to the presence of high-percentage phases like diopside (NAT-2: $CaMgSi_2O_6$, NAT-3: $(Mg_{0.964}Fe_{0.036})(Ca_{0.94}Na_{0.06})(Si_2O_6)$), and wollastonite (NAT-2, NAT-3: $CaSiO_3$). Additionally, neither the natural pigment

7

NAT-2 from Chile, nor the synthetic pigments contain chlorine. This is supported by literature [19].

Sample	Elemental Composition (at.%)							
	O	**Na**	**Mg**	**Al**	**Si**	**S**	**K**	**Ca**
SYN-1	60,6 - 63,1	2,9 - 13,4	3,5*	5,9 - 15,9	10,2 - 14,7	1 - 7,8	< 1	< 1*
SYN-2	52,2 - 63,7	<1 - 12,4		3,3 - 16,6	3,45 - 20,5	< 1 - 6,7	< 1 - 5,7*	< 1 - 34,1
SYN-3	60,4 - 62,7	6,6 - 12,5	1,5*	6,9 - 13,2	11,8 - 20,2	1,6 - 7,3	< 1	<1*
SYN-4	58,0 - 62,4	8,3 - 14,3	<1*	7,8 - 12,6	8,6 - 14,8	2,7 - 7,1	<1	<1*
SYN-5	59,9 - 67,0	4,4 - 14,0		2,5 - 14,9	2,5 - 16,3	2,2 - 16,2	<1	<1*
SYN-6	59,5 - 66,5	1,7 - 13,9	1,6*	2,9 - 16,6	3,2 - 17,8	<1 - 15,4	<1	<1 - 1,8
SYN-7	57,5 - 63,5	<1 - 13,4	<1*	7,6 - 16,8	10,9 - 18,4	<1 - 6,9	<1	<1
NAT-1	55,5 - 69,4	<1 - 13,0	< 1 - 10,1	<1 - 10,7	1,2 - 22,7	<1 - 18,6	<1 - 12,1	0 - 19,2
NAT-2	55,4 - 62,0	<1 - 13,3	<1 - 10,4*	<1 - 12,9	<1 - 22,2	<1 - 4,2	<1*	<1 - 35,1
NAT-3	40,2 - 62,7	<1 - 14,8		<1 - 12,3	4,3 - 20,6	<1 - 6,5	<1 - 1,2*	<1 - 16,8

Table 3: *EDS quantitative data (mean calculated values) of main elements for all the pigment samples. The "*" nomenclature indicates elements found in a single or a few grains in each sample.*

| Sample	Elemental Composition (at.%)											
	F	**Cl**	**Ti**	**Fe**	**Zr**	**Cr**	**V**	**P**	**Ni**	**Ce**	**Bi**	**Cu**
SYN-1				1,0*	7,6*							
SYN-2				< 1*								
SYN-3								2,1*	<1*			
SYN-4				<6,5*	5,1*				<1*			
SYN-5			<1*	<1 - 7,3*				<1*	<1*	<1*		
SYN-6				<1-6,9*				<1 - 2,3*	<1*	<1*		
SYN-7			<1 - 1*	<1 - 8,2*	<1*				<1*			<1*
NAT-1		< 1 - 1,9*	<1 - 4,1*	6,1 - 14,0*		< 1 - 4,6*	<1*					
NAT-2	8,3 - 10,4*		<1*	11,72 - 22,7*		5,6*		<1 - 14,7*	3,3*	<1*	2,0*	
NAT-3	1,7 - 26,3*	<1*		<1 - 22,9*								

Table 4: *EDS quantitative data (mean calculated values) of minor elements for all the pigment samples. The "*" nomenclature indicates that these minor elements were found in a single or a few grains in each sample.*

3.4 UV-Vis

3.4.1 UV-Vis diffuse reflectance spectroscopy

The UV–Vis diffuse reflectance spectra of all Ultramarine pigments are shown in Fig. 5. Due to factors impacting reflectance measurements, the diffuse reflectance spectra on pigments are typically more complicated, with relevant restrictions including variables like surface texture and roughness, particle size and distribution, and pigment compositional uniformity [20]. By identifying maximum peaks and inflection points, reflectance spectra can be utilized to distinguish between colorants with comparable colors [21]. In the present study, all pigments demonstrate a broad minimum at about 600 nm, which is in agreement with literature [21]. Synthetic pigments exhibit substantial absorption with low reflectivity intensity in this region of the spectrum (expect SYN-2), whereas natural pigments exhibit an increase in reflectivity intensity. Reinen et al. [22] claim that the S_3^- chromophore, which is trapped in the structural sodalite cages of lazurite, the primary crystalline phase of the pigments, is the cause of this absorption peak. Lazurite, being a member of the sodalite in the feldspathoids group, is a common phase rock in the crystalline

phases of Ultramarine, along with sodalite $Na_8[Al_6Si_6O_{24}]Cl_2$. The sodalites are a group of minerals that crystallize in succession in silicon and aluminum tetrahedra. These tetrahedra contain massive cubic and octahedral structures called "β cages" or "sodalite cages," which are similar to the structure of zeolites. In aluminosilicate matrix compositions that form tetrahedra of Al/SiO_4 inside the sodalite tetrahedron, the polysulfide chromophores (S_3^- for blue) are enclosed. As already mentioned by Aceto et al. [23] or M. Gargano et al. [24], there is a number of reasons that can cause this transition, including the admixture of blue pigment with a white material, like lead white. According to the current experimental results, the pigment SYN-2 provides the highest reflectivity at 600 nm. This pigment, the lightest of all the samples, contains $CaCO_3$, as it can be seen from the FTIR measurements and the XRD analysis.
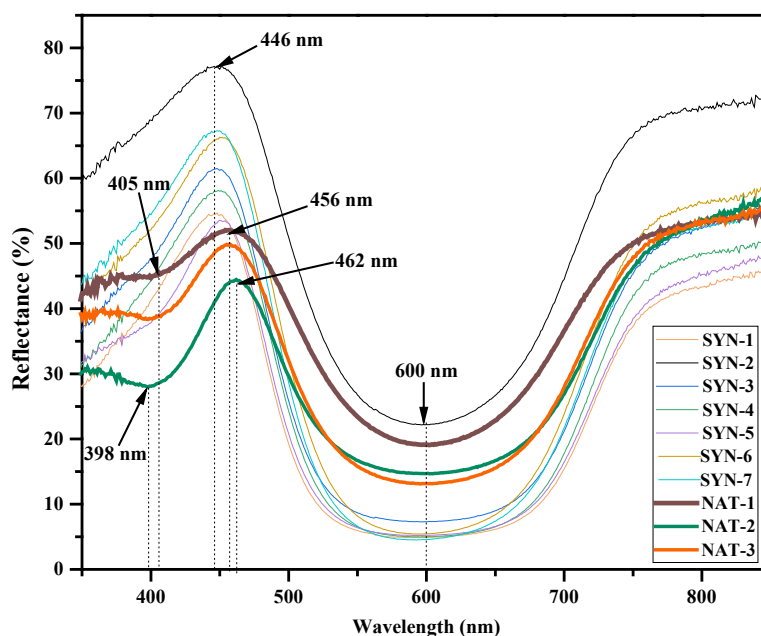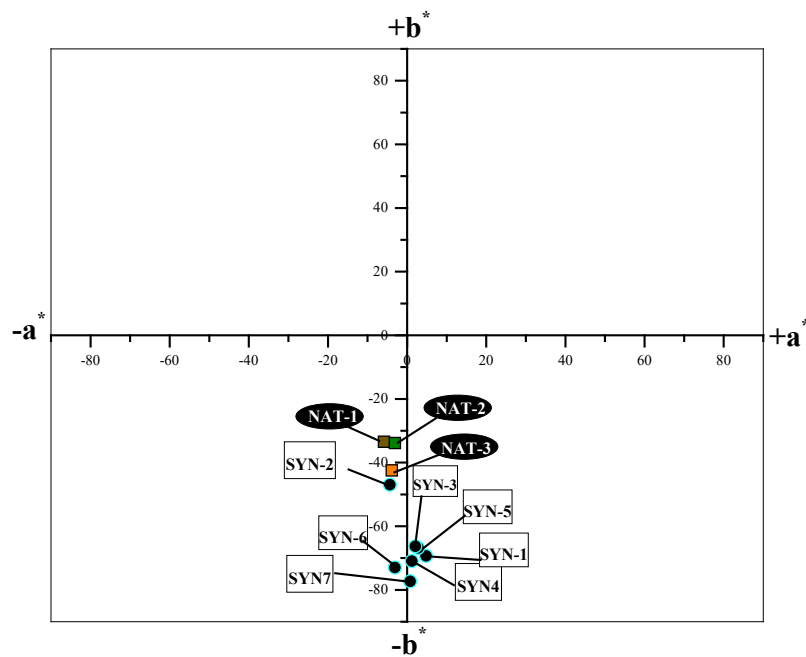

Figure 5: *Diffuse reflectance spectra of all the pigments under study. Thicker lines correspond to natural pigments, for comparative reasons.*

In the spectral region up to 450 nm, the two types of pigments differ further from one another (Fig. 5). In particular, natural pigments present their reflectance maxima at 456 nm for NAT-1 and at 462 nm for NAT-2, but the synthetic pigments have a reflectance maximum at 446 nm. Also, the pigments NAT-1 and NAT-3 have a reflectance minimum at 405 nm, while NAT-2 exhibits this minimum at 398 nm. According to Bacci et al. [25], these variations are caused by the contribution of additional chromophores that present overlapping absorption bands, with the natural pigment sample from Chile having the strongest one.

3.4.2 Colorimetry

Each diffuse reflectance spectrum of the Ultramarine pigments was transformed to the CIELAB (Commission Internationale de l'Eclairage) color space system, using the colorimetric parameters a* (from negative values representing color green, up to positive values representing color red), and b* (from negative values represent color blue, up to positive values representing

color). The parameter L* expresses the color's brightness, or how well the sample can reflect or absorb some of the light that strikes it (L* is equal to 100 for white samples and 0 for black samples) [26]. In particular, the parameters L*, a*, b* are calculated based on the X, Y, Z trichromatic values derived from a linear transformation of the RGB system, due to the fact that, the spectral reflection coefficient is calculated for wavelengths between 380 nm and 780 nm. Depending on the reference, the axes a* and b* are infinite and white can easily surpass ±150. In the present study, L* values were excluded, as the measurements were conducted to samples prepared by pilling and spreading a small amount of each pigment on a layer of compressed BaSO$_4$; this resulted to inhomogeneous specimens in terms of brightness. Figure 6 clearly shows that the blue zone is where the majority of synthetic pigments are located. The lightest synthetic pigment SYN-2 which is located toward the edges of the blue zone, is grouped with the natural pigments, which are all grouped together.

Figure 6: *Color characterization of the pigments in the CIELAB color space using color parameters a* and b**

3.4.3 Optical band gap estimation of pigments

UV-Vis diffuse reflectance spectroscopy can be used for studying the band gap behavior of materials. An increase in absorbance or reflectance at a specific wavelength indicates that the electrons have been optically excited to move from the valence band into the conduction band (band gap energy) [27]. The Kubelka-Munk theory (1931) was developed to explain the transport of radiation by considering the multiple scattering that occurs when radiation is reflected, transmitted and absorbed by a surface. With this method we can calculate -with relative accuracy- the reflectivity of a surface of any material [28]. The Kubelka-Munk theory is based in the following equation:

$$F(R) = \frac{(1-R)^2}{2R}$$

Eq. 1

where R is the reflectance. In this study, the optical band gap (E_g) estimation of the pigments (Figs 7 & 8) was obtained by applying the corresponding Tauc plots, using the general equation:

$$a(hv) \approx B(hv - Eg)^n \text{ (where } a{\sim}F(R))$$ *Eq. 2*

where *a* is the extinction coefficient (proportional to *F(R)*), *n* is the corresponding coefficient associated with an electronic transition, with *n* = 1/2 for a direct allowed transition and *n* = 2 for an indirect allowed transition [27, 29, 30], *h* is the Planck's constant, *v* is the frequency, and *B* is the absorption constant. It should be noted that the Kubelka-Munk theory offers an approximation to attain quantitative information from diffuse reflectance measurements [20], through which E_g values can be evaluated [27]. On this direction, although the application of the Tauc plot method may present uncertainty, it is very simple to be applied, and it has been demonstrated that it gives uncertainty of ~1% of the E_g value [27, 31, 32, 33]. Applying Equations 1 & 2 to the reflectance data of all the pigments under study, the corresponding results are shown in Table 5. In both cases, the E_g values do not lead to differentiation between synthetic and pigments of natural origin.

Sample	Direct Band gap (eV)		Indirect Band gap (eV)		
SYN-1	1,8	4,1	1,6	2,4	3,5
SYN-2	1,8	4,2	1,6	2,3	3,5
SYN-3	1,8	4,1	1,6	2,4	3,5
SYN-4	1,8	4,1	1,6	2,4	3,5
SYN-5	1,8	4,1	1,6	2,4	3,5
SYN-6	1,8	4,2	1,6	2,3	3,7
SYN-7	1,8	4,2	1,6	2,4	3,7
NAT-1	1,8	4,1	1,5	1,8	3,2
NAT-2	1,7	4,0	1,6	2,3	3,2
NAT-3	1,8	4,1	1,6	2,2	3,5

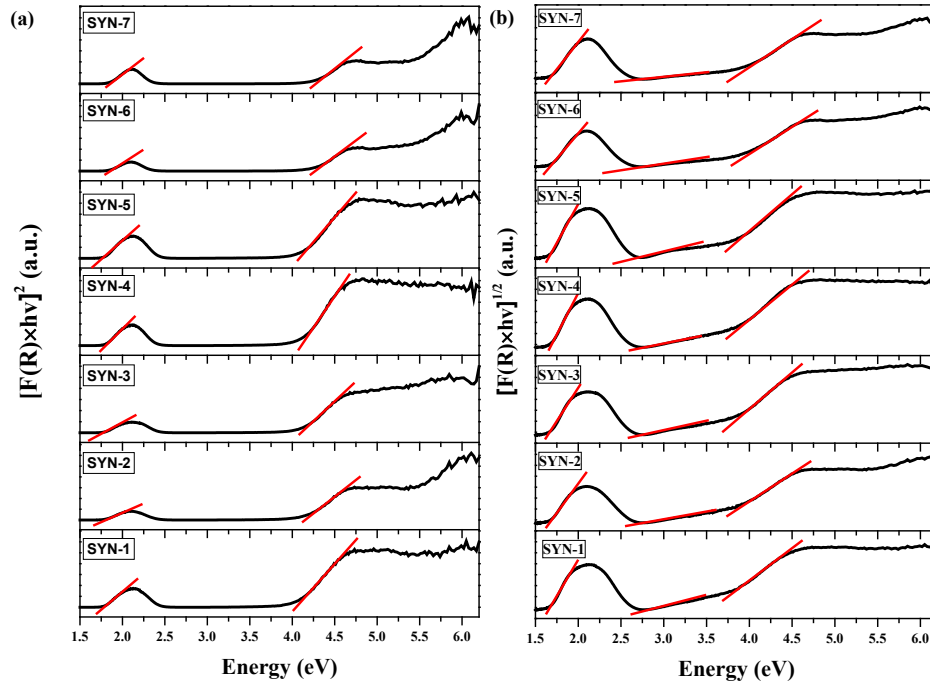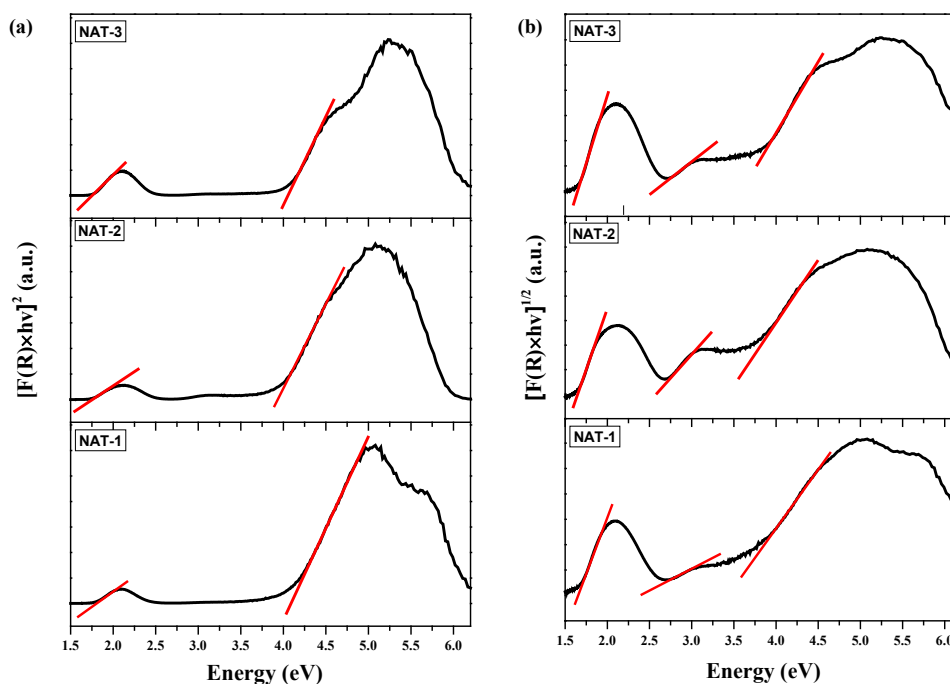**Table 5:** *Experimental E_g values of the Ultramarine pigments*

Figure 7: *Tauc plots of the synthetic Ultramarine pigments for the determination of their direct (a) and the indirect optical band gaps.*

11

Figure 8: *Tauc plots of the natural Ultramarine pigments for the determination of their direct (a) and the indirect optical band gaps.*

4.   Conclusions

In this research work, ten samples of commercially available natural and synthetic Ultramarine pigments were used to investigate the possibility of their discrimination using characterization methods. FTIR spectra showed that the slight differences between the spectra of the natural and synthetic ultramarines are related to the presence of other components, such as kaolinite in the synthetic pigments, whereas in the natural pigments, the S_3^- chromophore's difficulty to be discriminated is evident. In general, all spectra are characterized by the presence of aluminosilicates.

The differences between natural and synthetic Ultramarine pigments are directly distinguished by the contained crystalline phases through XRD. While lazurite is identified in every case, all synthetic pigments contain the additional phases of haüyne, kaolinite and muscovite. On the other hand, the latter are absent in the natural pigments; in this case -and apart from lazurite-, diopside and sodalite characterize the natural pigments. Moreover, wollastonite is present in the natural ones of American origin, while phlogopite is found only in the natural one that originates from Afghanistan.

For the morphological examination and elemental analysis of all samples, SEM-EDS analysis was applied. The pigments' morphology indicated that the synthetic pigments are composed of homogeneous in dimensions spherical grains, while the natural ones present grains of sharper edges and inhomogeneity in dimensions. According to the elemental analysis, sodium, aluminum, silicon, and sulfur are the primary components of both synthetic and natural pigments. Furthermore, additional elements like fluorine, magnesium, chlorine, titanium, and iron were included in natural pigments. These additional elements are correlated to the crystal phases diopside, wollastonite, sodalite, and phlogopite.

As said, by identifying maximum peaks and inflection points, which correspond to maxima or minima in the UV-Vis diffuse reflectance spectra, can lead to distinguish between pigments with comparable hues. All the UV-Vis reflectance spectra display a reflectance minimum at 600 nm, which is attributed to the S_3^- chromophore, entrapped in the structural sodalite cages of lazurite. The two types of pigments diverge much more from one another in the two zones with the highest reflections, at 400 and 450 nm. In order to demonstrate the color variations observed among the samples, CIELAB parameters a* and b* indicate that natural pigments present a clustering. Finally, the calculated optical band gaps of the pigments show that no distinction can be achieved.

References

[1] J. Plesters, *Ultramarine blue, natural and artificial.* In: Roy Ashok, editor. Artists' Pigments A Handbook of their History & Characteristics. (1993) p. 1–232.

[2] D. Reinen, G.-G. Lindner, *The nature of the chalcogen colour centres in ultramarine-type solids*, Chem. Soc. Rev. 28 (1999) 75–84.
[doi:10.1039/A704920J]

[3] C.M. Schmidt, M.S. Walton, K. Trentelman. *Characterization of lapis lazuli pigments using a multitechnique analytical approach: implications for identification and geological provenancing.* Anal Chem 81 (2009) 8513–8.
[doi:10.1016/j.culher.2008.12.001]

[4] M. González-Cabrera et al., *Natural or synthetic? Simultaneous Raman/luminescence hyperspectral microimaging for the fast distinction of ultramarine pigments*, Dyes Pigm. 178 (2020) 108349.
[doi:10.1016/j.dyepig.2020.108349]

[5] M. Favaro, A. Guastoni, et al. *Characterization of lapis lazuli and corresponding purified pigments for a provenance study of ultramarine pigments used in works of art.* Anal Bioanal Chem 402 (2012) 2195–208.
[doi: 10.1007/s00216-011-5645-4]

[6] M.R. Derrick et al. *Infrared Spectroscopy in Conservation Science*. Getty Conservation Institute 1999.

[7] C. Miliani, A. Daveri, et al. *CO_2 entrapment in natural ultramarine blue*. Chemical Physics Letters, 466(4-6) (2008) 148–151.
[doi:10.1016/j.cplett.2008.10.038]

[8] G.D. Smith, R.J. Klinshaw. *The presence of trapped carbon dioxide in lapis lazuli and its potential use in geo-sourcing natural ultramarine pigment.* J Cult Herit 10 (2009) 415–21.
[doi:10.1016/j.culher.2008.12.001]

[9] Kremer Pigments GmbH & Co. KG, https://www.kremer-pigmente.com/

[10] B.J. Saikia, G. Parthasarathy. *Fourier Transform Infrared Spectroscopic Characterization of Kaolinite from Assam and Meghalaya, Northeastern India*. Journal of Modern Physics, 01(04) (2010) 206–210.
[doi:10.4236/jmp.2010.14031]

[11] E. Cato, A. Rossi, N.C. Scherrer, E.S.B. Ferreira. *An XPS study into sulphur speciation in blue and green ultramarine*. Journal of Cultural Heritage 29 (2018) 30–35.
[doi.org/10.1016/j.culher.2017.09.005]

[12] V. Desnica, K. Furic, M. Schreiner. *Multianalytical characterization of a variety of ultramarine pigments*, e-Preservation Science 1 (2004): 15-21.

[13] D. Shan, S. Wang et al. *Direct electrochemistry and electrocatalysis of hemoglobin entrapped in composite matrix based on chitosan and $CaCO_3$ nanoparticles*. Electrochemistry Communications, 9(4) (2007) 529–534.
[doi:10.1016/j.elecom.2006.10.032]

[14] M. T. D. Carbó, F. B. Reig, et al. *Fourier transform infrared spectroscopy and the analytical study of works of art for purposes of diagnosis and conservation*. Analytica Chimica Acta, 330 (2-3) (1996) 207–215.
[doi:10.1016/0003-2670(96)00177-8]

[15] C. Hubbard, R. Snyder. *RIR - Measurement and Use in Quantitative XRD*. Powder Diffraction, 3(2) (1998) 74-77.
[doi:10.1017/S0885715600013257]

[16] JCPDS-ICDD, PC Powder Diffraction Files, (2003)

[17] C.M. Schmidt, M.S. Walton, K. Trentelman. *Characterization of Lapis Lazuli Pigments Using a Multitechnique Analytical Approach: Implications for Identification and Geological Provenancing.* Analytical Chemistry, 81(20) (2009) 8513–8518.
[doi: 10.1021/ac901436g]

[18] S. Fernández-Sabido, Y. Palomo-Carrillo, et al. *Comparative Study of Two Blue Pigments from the Maya Region of Yucatan.* MRS Proceedings, 1374 (2012) 115–123.
[doi: 10.1557/opl.2012.1382]

[19] S.M. Aleksandrov, V. G. Senin. *Genesis and composition of lazurite in magnesian skarns.* Geochemistry International, 44(10) (2006) 976–988.
[doi: 10.1134/S001670290610003X]

[20] M. Picollo, M. Aceto, T. Vitorino. *UV-Vis spectroscopy. Physical Sciences Reviews* 4 (2019) 20180008.
[doi: 10.1515/psr-2018-0008]

[21] M. Aceto, A. Agostino, et al. *Characterisation of colourants on illuminated manuscripts by portable fibre optic UV-visible-NIR reflectance spectrophotometry.* Analytical Methods, 6(5) (2014) 1488.
[doi:10.1039/C3AY41904E]

[22] D. Reinen, G.-G. Lindner. *The nature of the chalcogen colour centres in ultramarine-type solids.* Chemical Society Reviews, 28(2) (1999) 75–84.
[doi:10.1039/A704920J]

[23] M. Aceto, A. Agostino, et al. *Non-invasive differentiation between natural and synthetic ultramarine blue pigments by means of 250–900 nm FORS analysis.* Analytical Methods, 5(16) (2013) 4184.
[doi:10.1039/C3AY40583D]

[24] M. Gargano, N. Ludwig, et al. *Variazioni dello spettro di riflettanza di pigmenti in miscele di pigmenti antichi,* in Proceedings of the IV Congresso Nazionale di Archeometria, ed. C. Arias and M. P. Colombini, ETS, Pisa, 2006.

[25] M. Bacci, C. Cucci, et al. *An integrated spectroscopic approach for the identification of what distinguishes Afghan lapis lazuli from others.* Vibrational Spectroscopy, 49 (2009) 80–83.
[doi:10.1016/j.vibspec.2008.05.002]

[26] O. Noboru and A. Robertson, Colorimetry, *Fundamentals and Applications.* John Wiley & Sons Inc. Editions, USA, 2006.
[doi:10.1002/0470094745.ch2]

[27] R. López, R. Gómez. *Band-gap energy estimation from diffuse reflectance measurements on sol–gel and commercial TiO$_2$: a comparative study.* Journal of Sol-Gel Science and Technology, 61 (2011) 1–7.
[doi: 10.1007/s10971-011-2582-9]

[28] P. Kubelka, F. Munk. *An article on optics of paint layers.* Z. Tech. Phys 12.593-601 (1931): 259-274.

[29] M.A. Blesa. Eliminación De Contaminantes Por Fotocatálisis Heterogénea. CYTED 2001.

[30] B. Brunetti, C. Miliani, et al. *Non-invasive Investigations of Paintings by Portable Instrumentation: The MOLAB Experience.* In: Mazzeo, R. (eds) Analytical Chemistry for Cultural Heritage. Topics in Current Chemistry Collections. Springer, Cham. 2017.
[doi: 10.1007/s41061-015-0008-9]

[31] T. Illés, J. Mayer, T. Terlaky. *Pseudoconvex optimization for a special problem of paint industry,* Eur. J. Oper. Res. 79 (1994) 537–548.
doi:10.1016/0377-2217(94)90064-7.

[32] J. Torrent, V. Barrón, *Diffuse Reflectance Spectroscopy*, in: Methods Soil Anal., Soil Science Society of America Journal, 2008: pp. 367–385.

[33] B.D. Viezbicke, S. Patel, B.E. Davis, D.P. Birnie, *Evaluation of the Tauc method for optical absorption edge determination: ZnO thin films as a model system*, Phys. Status Solidi Basic Res. 252 (2015) 1700–1710.
doi:10.1002/pssb.201552007.